Supplement of Atmos. Chem. Phys., 26, 13227–13252, 2026
https://doi.org/10.5194/acp-26-13227-2026-supplement

Atmospheric Chemistry and Physics
Open Access
EGU

Supplement of

Chemical characterization and source apportionment of carbonaceous aerosols during post-monsoon biomass burning and Diwali at an upwind site of Delhi

Vasu Singh et al.

Correspondence to: Vasu Singh (vasu.singh@cas.iitd.ac.in)

Contents of this file

This supporting information contains 3 sections, 17 additional Figures (S1-S17) and 5 Tables (S1-S5) in 29 pages.

S1. Positive Matrix Factorization Analysis

Positive Matrix Factorization was applied to the organic aerosol mass spectra measured by the ToF-ACSM at Sonipat to resolve the major OA factors contributing during the campaign. The analysis was performed using the Source Finder software, SoFi, with the multilinear engine ME-2 (Paatero and Tapper, 1994; Ulbrich et al., 2009). We followed the general PMF evaluation framework described by (Canonaco et al., 2021), including factor-number exploration, evaluation of rotational ambiguity, constrained-profile sensitivity, bootstrap resampling, and residual analysis.

Optimal factor solution

We tested PMF solutions containing three to seven factors for the complete campaign dataset. The factor number was evaluated using changes in Q/Q_{exp}, where Q is the uncertainty-weighted sum of the squared differences between the measured and modelled data and Q_{exp} is its statistically expected value based on the number of data points and fitted parameters. A substantial decrease in Q/Q_{exp} after adding a factor indicates an improvement in model fit, whereas a comparatively small decrease suggests that the additional factor provides limited explanatory value. Because Q/Q_{exp} generally decreases as more factors are added, it was not used as the sole criterion for selecting the solution.

The five-factor solution was selected based on the elbow in the Q/Q_{exp} scree plot, improvements in the residual structure from four to five factors, the chemical interpretability of the factor profiles, distinct temporal behavior, correspondence with independent tracers, and the absence of meaningful additional source information in the higher-order solutions (Fig. S1). Increasing the number of factors, solutions produced splitting of existing factors or additional profiles that were not sufficiently distinct in their mass spectra and time series. Taken together, these diagnostics supported selection of a five-factor structure.

The unconstrained five-factor solution nevertheless showed substantial mixing between HOA and SFCOA, which is a recognized challenge in environments influenced simultaneously by fossil-fuel and solid-fuel combustion. Therefore HOA reference profile from Canonaco et al., (2013) and Crippa et al., (2013) was constrained using random a-values approach between 0 and 0.5. This approach allowed the HOA profile to vary from the reference spectrum while improving the separation and chemical interpretability of HOA and SFCOA. All other factors were allowed to evolve without profile constraints.

The selected solution was evaluated using the following complementary criteria.

Temporal patterns: Factor time series and diurnal profiles were examined for physically interpretable and distinct temporal patterns. Strongly correlated profiles with similar time series were treated as possible evidence of factor splitting rather than as independent sources (Figs. S2 and S3).

Mass spectra: Each factor's mass spectrum was inspected for chemically interpretable features and characteristic marker ions and compared against known OA source profiles from the literature and reference spectra from the AMS/ACSM spectral database (https://cires1.colorado.edu/jimenez-group//AMSsd/) and Datalystica database to aid source identification.

Relationships with independent variables: Factor time series were compared with non-refractory inorganic aerosol species measured by the ToF-ACSM, equivalent black-carbon components, available gaseous tracers, and meteorological variables. These comparisons were used as supporting evidence for factor interpretation rather than as unique source-identification criteria (Figs. S4-S7).

Rotational and constraint sensitivity: FPEAK values from -1.0 to $+1.0$, at intervals of 0.2, were explored for the tested factor solutions. For the five-factor solution, the minimum Q/Q_{exp} was 9.17 at FPEAK $= -0.2$. The variation in Q/Q_{exp} across the tested FPEAK range remained within the predefined 10% range of the minimum value. This result indicates limited sensitivity of the overall model fit to rotational forcing within the explored FPEAK interval. The selected solution was also evaluated for changes in factor profiles, time series, and mass contributions rather than from Q/Q_{exp} alone.

The sensitivity of the HOA–SFCOA separation to the applied HOA constraint was evaluated by varying the HOA a-value between 0 and 0.5. The resulting HOA and SFCOA profiles and mass contributions showed limited variation across the tested range, indicating that the reported source apportionment is not strongly sensitive to the exact a-value chosen within this bound (Fig. S8). Across the HOA a-value sensitivity analysis, the factor contributions remained within 7-9% for HOA, 21-26% for SFCOA, 10-14% for BBOA, 18-20% for LO-OOA, and 36-40% for MO-OOA, without a systematic redistribution between HOA and SFCOA

Bootstrap Analysis: Bootstrap resampling was used to evaluate the statistical reproducibility of the final HOA-constrained five-factor solution. A total of 500 resampled datasets were analysed in SoFi using the same factor configuration and constraint settings as the base solution. Factors from each bootstrap run were mapped to the corresponding base-case factors using the correlation-based criteria, following Canonaco et al., 2021; Chen et al., 2022 and Ulbrich et al.,

2009. A bootstrap run was classified as successful only when all five factors satisfied the defined mapping criteria.

Of the 500 bootstrap runs, all the 500 runs successfully reproduced all five factors, corresponding to a successful mapping rate of 100**%**. These results indicate the extent to which the five-factor solution was reproducible under resampling.

Residual analysis: The quality of the final five-factor model fit was further evaluated using the uncertainty-scaled residuals. The median residual as a function of m/z remained close to zero for most fitted ions, indicating no persistent positive or negative bias in the reconstruction of the mass spectra (Fig. S9a). Residuals as a function of time were also generally centred near zero, although several short periods showed a broader residual distribution (Fig. S9b). These intervals may reflect rapid changes in aerosol composition, unrepresented short-lived sources, or measurement uncertainties that were not fully captured by the error model.

Overall, these results indicate an adequate and unbiased model fit across both the temporal and mass spectral dimensions. The distribution of scaled residuals was approximately Gaussian and centered close to zero (mean ≈ 3×10^{-6}; Gaussian fit center = -0.15, width = 3.52), indicating no systematic bias in the model fit (Figure S9c).

S2.Estimation of elemental ratios for the PMF factors

The oxygen-to-carbon and hydrogen-to-carbon ratios of the PMF-resolved organic aerosol factors were estimated from their unit-mass-resolution mass spectra rather than measured directly from high-resolution elemental ion signals. For each normalized factor profile, f_{44} and f_{43} were defined as the fractions of the total organic signal occurring at $m/z44$ and m/z 43, respectively:

$$f_{44} = \frac{I_{44}}{\sum_m I_m} \quad \text{(S1)}$$

$$f_{43} = \frac{I_{43}}{\sum_m I_m} \quad \text{(S2)}$$

where I_m is the organic signal at nominal mass-to-charge ratio m.

Initial elemental-ratio estimates were calculated using the Improved-Ambient parameterizations developed by Canagaratna et al. (2015):

$$\text{O:C}_{\text{IA}} = 0.079 + 4.31 f_{44} \quad \text{(S3)}$$

$$\text{H:C}_{\text{IA}} = 1.12 + 6.74 f_{43} - 17.77 f_{43}^2 \quad \text{(S4)}$$

These relationships (Eq. (S3) and Eq. (S4)) were originally developed primarily using standard-vaporizer AMS measurements. Because the ToF-ACSM used in the present study was equipped with a capture vaporizer, which produces greater thermal decomposition and different organic fragmentation patterns, the capture-vaporizer calibration factors reported by Hu et al., (2018) for ambient OA were applied. The corrected ratios were calculated as:

$$\text{O:C}_{\text{CV}} = 0.73\ \text{O:C}_{\text{IA}} = 0.73(0.079 + 4.31 f_{44}) \quad \text{(S5)}$$

$$\text{H:C}_{\text{CV}} = 0.72\ \text{H:C}_{\text{IA}} = 0.72(1.12 + 6.74 f_{43} - 17.77 f_{43}^2) \quad \text{(S6)}$$

This procedure was applied separately to the representative mass spectrum of each PMF-resolved factor. The resulting O:C and H:C estimates are reported in Table S1 (using Eq. (S5) and Eq. (S6)) and were used to compare the relative degree of oxygenation among the factors.

These values are subject to uncertainty and should not be interpreted as direct measurements of elemental composition. The f_{44}-based O:C relationship has reduced accuracy for primary OA components with low f_{44}, particularly when f_{44} is below approximately 0.04 (Canagaratna et al., 2015). In addition, capture-vaporizer fragmentation can affect the signals used in the

parameterizations. Hu et al., (2018) estimated uncertainties of approximately 23% for O:C and 18% for H:C for standard organic compounds measured using a capture-vaporizer AMS. The ratios reported here (using Eq. (S5) and Eq. (S6)) are therefore treated as approximate indicators of relative oxidation state, particularly for the HOA, BBOA, and SFCOA factors, rather than as precise quantitative elemental compositions.

S3. Sensitivity of Aethalometer-model BC source apportionment to assumed AAE values:

The Aethalometer model requires prescribed absorption Ångström exponents for fossil-fuel-related and biomass-burning-related aerosol absorption. As these exponents vary with fuel type, combustion conditions, particle mixing state, atmospheric processing, and the contribution of brown carbon, their assumed values represent an important source of uncertainty in the calculated eBC source fractions.

For the reference source-apportionment analysis, we used $\alpha_{\mathrm{ff}} = 1.0$ and $\alpha_{\mathrm{bb}} = 2.0$ for the 470 and 950 nm wavelength pair. These values are widely used in Aethalometer-model studies and lie within the ranges commonly reported for fossil-fuel and biomass or solid-fuel combustion aerosols. However, they are treated here as reference values rather than as uniquely constrained site-specific exponents.

We evaluated the sensitivity of the source apportionment by repeating the calculations for α_{ff} values of 0.9, 1.0, and 1.1 and α_{bb} values from 1.7 to 2.2 at intervals of 0.1. Figure S10 shows the resulting variation in the eBC_{ff} and eBC_{bb} fractions. Across the tested combinations, the arithmetic mean of the time-resolved eBC_{ff}/eBC fraction ranged from 20.3% to 61.6%, while the corresponding eBC_{bb}/eBC fraction ranged from 38.4% to 79.7%.

The model results were more sensitive to α_{bb} than to α_{ff}. At a fixed α_{ff} of 1.0, the mean eBC_{ff} fraction increased from 22.4% to 58.2% as α_{bb}increased from 1.7 to 2.2. In contrast, at a fixed α_{bb} of 2.0, the mean eBC_{ff} fraction increased from 43.6% to 49.9% as α_{ff} increased from 0.9 to 1.1. These results demonstrate that the quantitative source split, particularly the biomass or solid-fuel fraction, depends strongly on the assumed biomass-burning AAE.

At the reference combination of $\alpha_{\mathrm{ff}} = 1.0$and $\alpha_{\mathrm{bb}} = 2.0$, the arithmetic means of the time-resolved eBC_{bb}/eBC and eBC_{ff}/eBC fractions were 53.6% and 46.4%, respectively. These values differ from the campaign mass-weighted fractions calculated from the ratio of the campaign-mean concentrations. The mean concentrations of eBC_{bb} and eBC_{ff} were 10.9 and 3.1 μg m^{-3}, corresponding to mass-weighted fractions of 77.8% and 22.2%. The difference arises because the mass-weighted calculation gives greater weight to high-eBC periods, during which the model indicated a stronger biomass or solid-fuel optical contribution.

The sensitivity results indicate that the Aethalometer model provides evidence for an important biomass or solid-fuel influence, particularly during high-loading periods, but the exact numerical source split remains uncertain. In addition, eBC_{bb} is an operational optical category and may include crop-residue burning, wood combustion, dung burning, and other brown-carbon-rich solid-fuel sources. It should not be interpreted as a unique measure of agricultural residue burning. Independent source constraints, such as radiocarbon measurements or source-specific tracer observations, would be required for a more definitive separation of fossil and non-fossil combustion contributions.

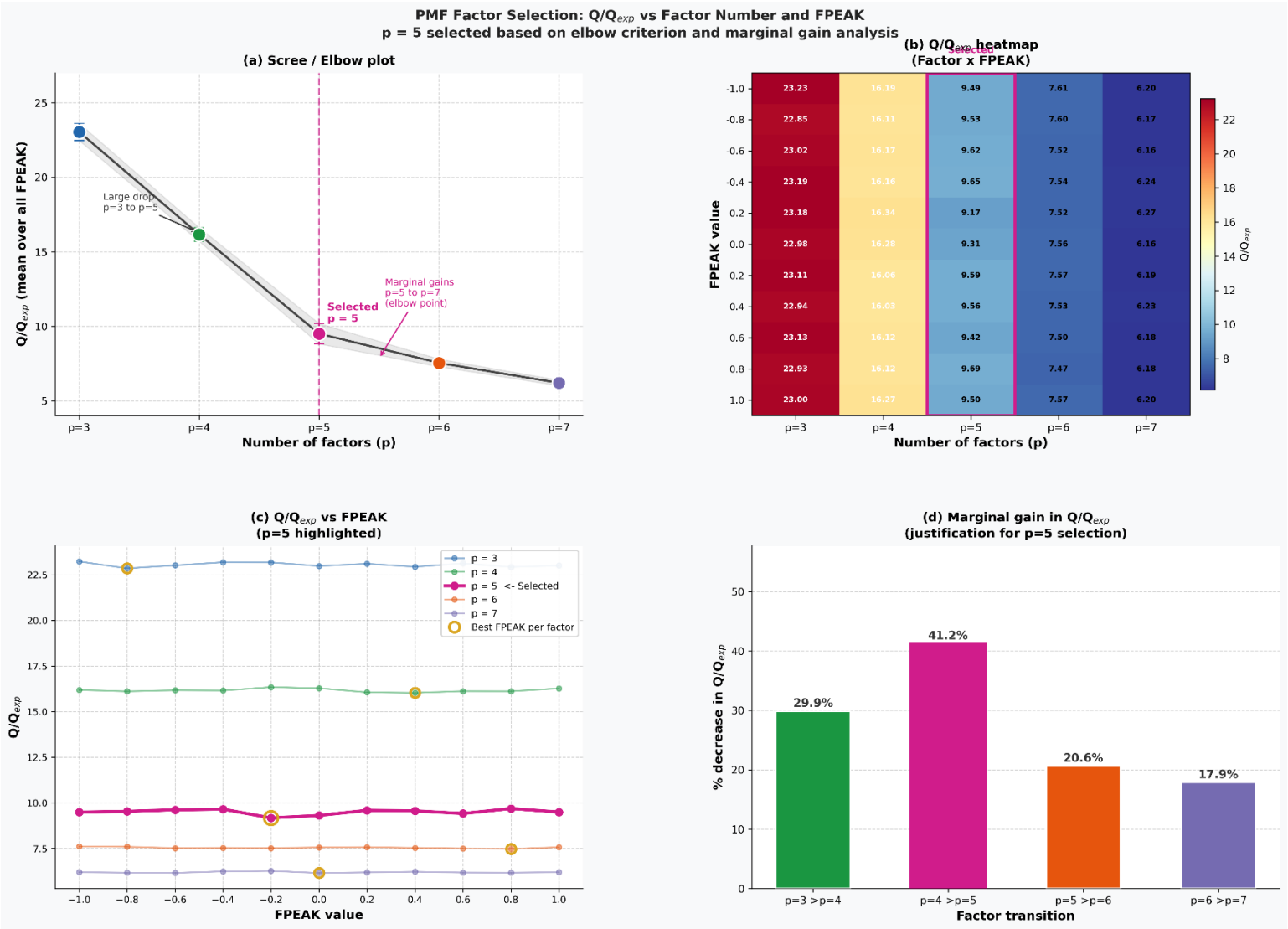

***Figure S1**: Q/Qexp as a function of factor number (p = 3-7) and FPEAK value (-1.0 to 1.0), showing (a) the scree/elbow plot, (b) a heatmap across factor number and FPEAK, (c) Q/Qexp versus FPEAK for each factor solution, and (d) the percentage decrease in Q/Qexp at each factor-number transition.*

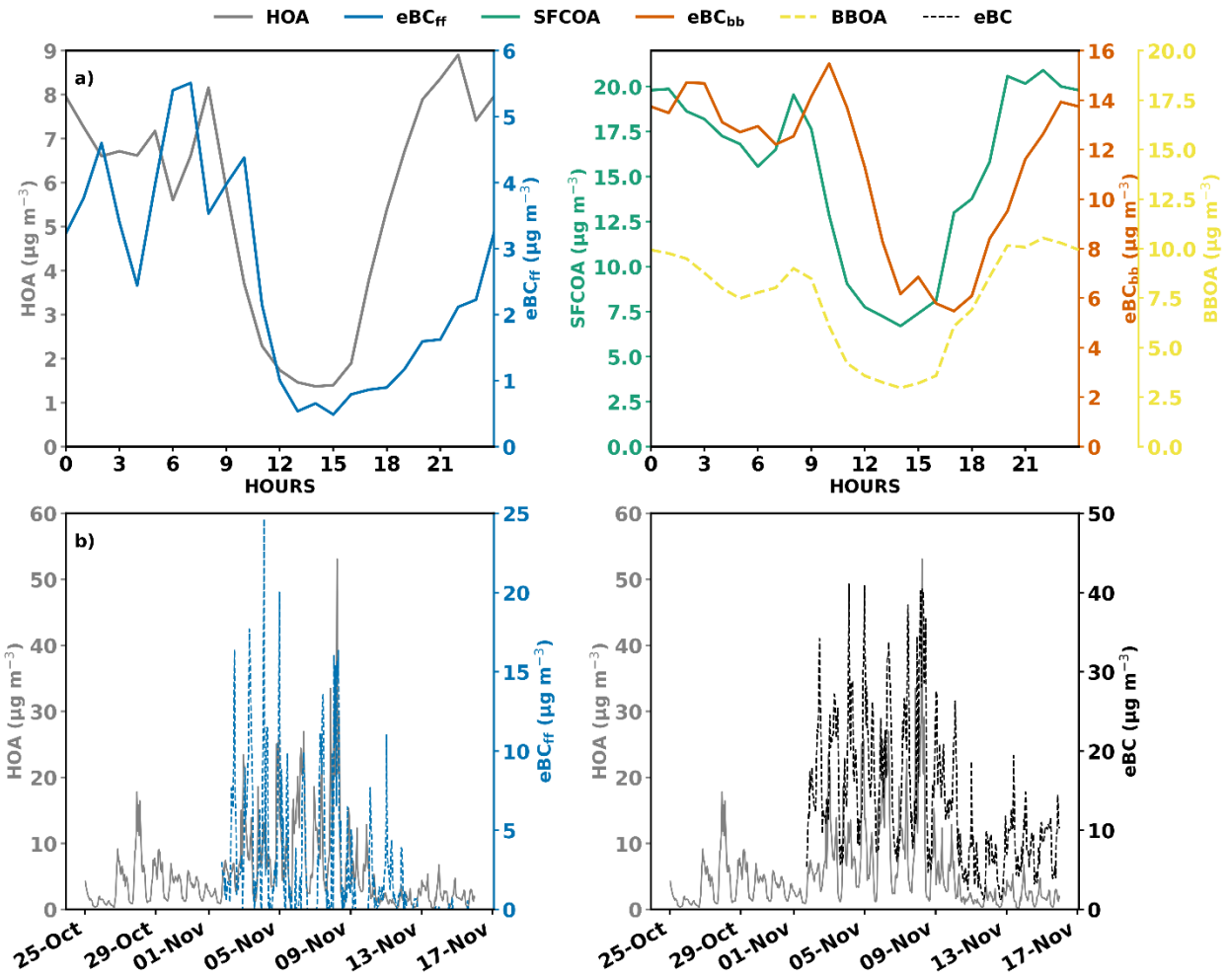

Figure S2: *Comparison of PMF-resolved organic aerosol factors with Aethalometer-derived eBC components. (a) Mean diurnal concentrations of HOA and eBC_{ff} during the biomass-burning period. (b) Mean diurnal concentrations of SFCOA, BBOA, and eBC_{bb} during the same period. (c) Temporal variations of HOA and eBC_{ff}. (d) Temporal variations of HOA and total eBC. Separate vertical axes are used for the different components because of their differing concentration ranges. Diurnal profiles are shown in local time.*

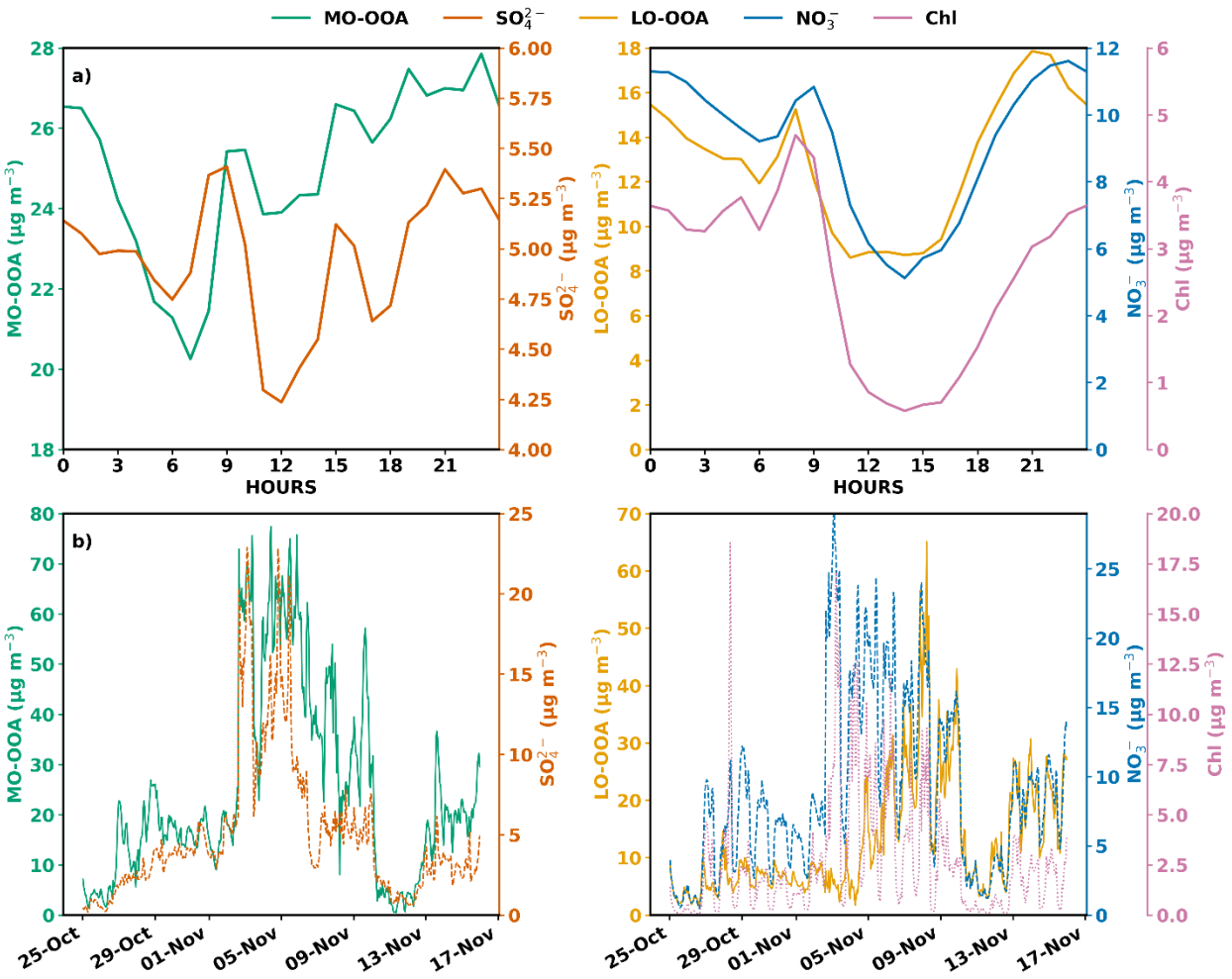

Figure S3: *a) Mean diurnal mass concentrations for the Biomass Burning period. Additionally, the diurnal profiles of SO_4^{2-}, NO_3^- and Chl^- are shown with the corresponding ACSM factors. b) Temporal trends of factors LO-OOA and MO-OOA with SO_4^{2-}, NO_3^- and Chl^-.*

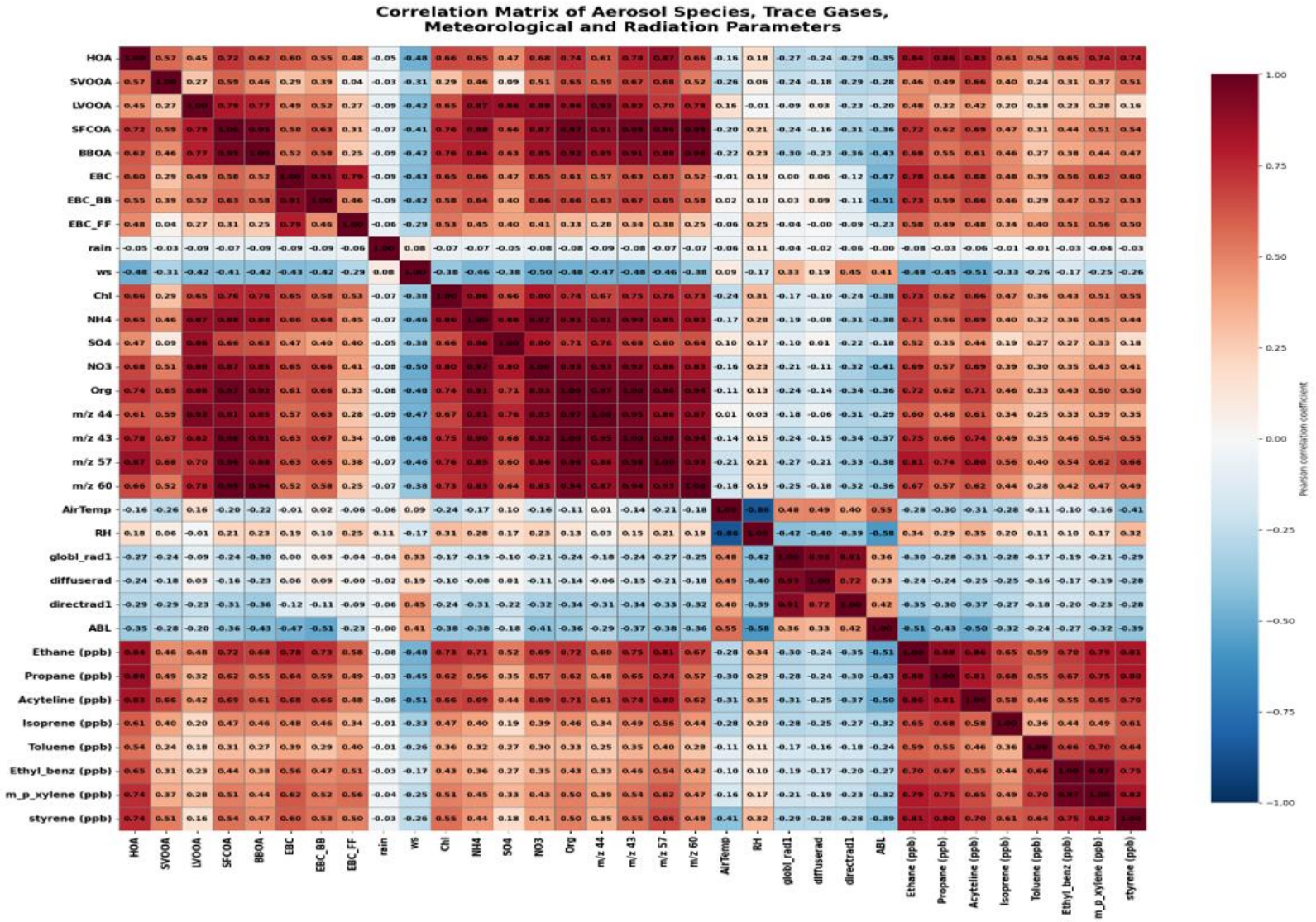

Figure S4: *Correlation (Pearson R) of PMF factors: HOA, LO-OOA, MO-OOA, SFCOA and BBOA with $PM_{2.5}$ species, gases and meteorology for data acquired from 25th October 2023 to 15th November 2023.*

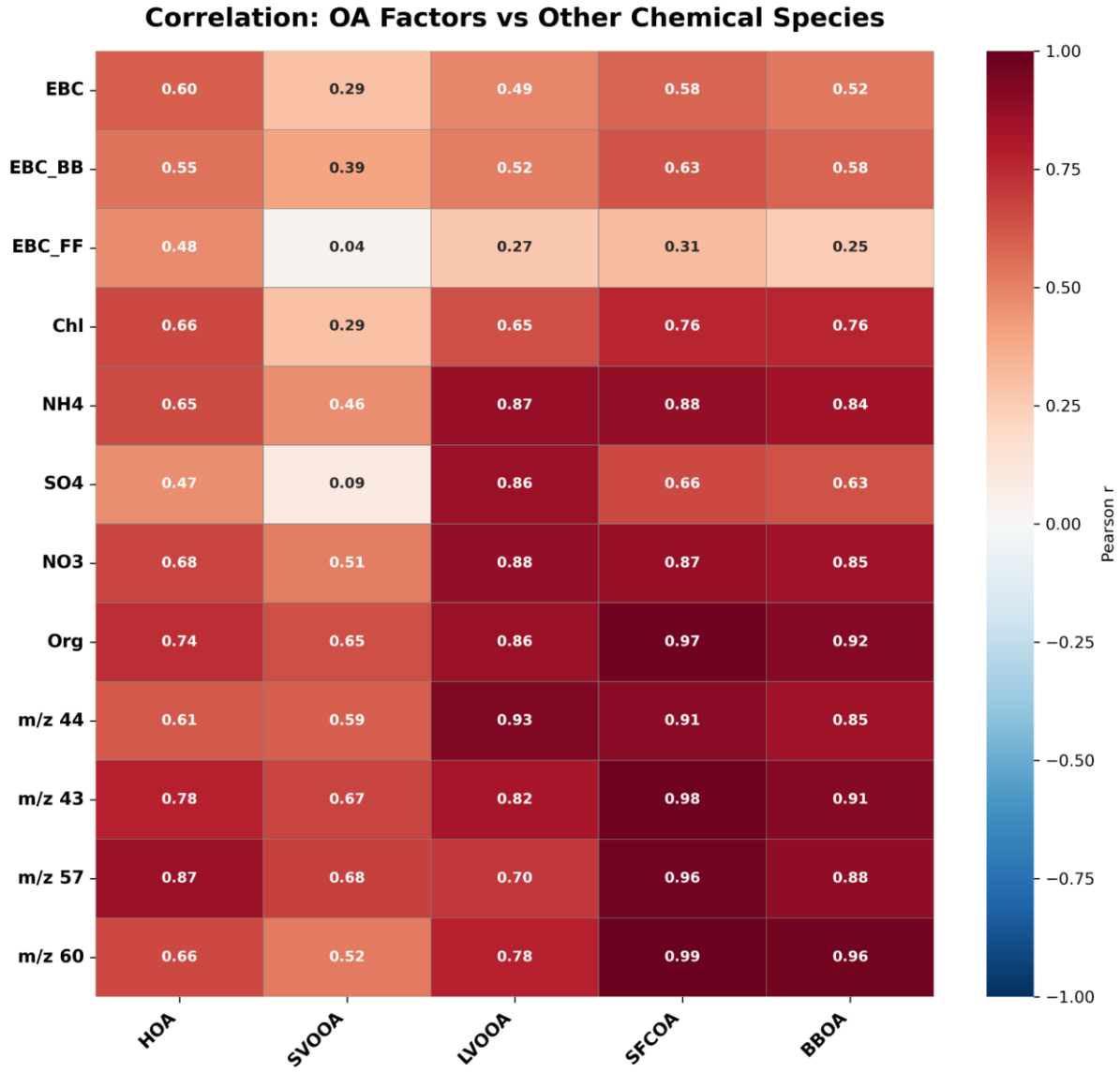

Figure S5: *Pearson correlation heatmap between organic aerosol (OA) factors (HOA, LO-OOA, MO-OOA, SFCOA, BBOA) and other chemical species, including black carbon components, inorganic ions, bulk organics, and ACSM marker fragments. Colors represent the strength and direction of correlations.*

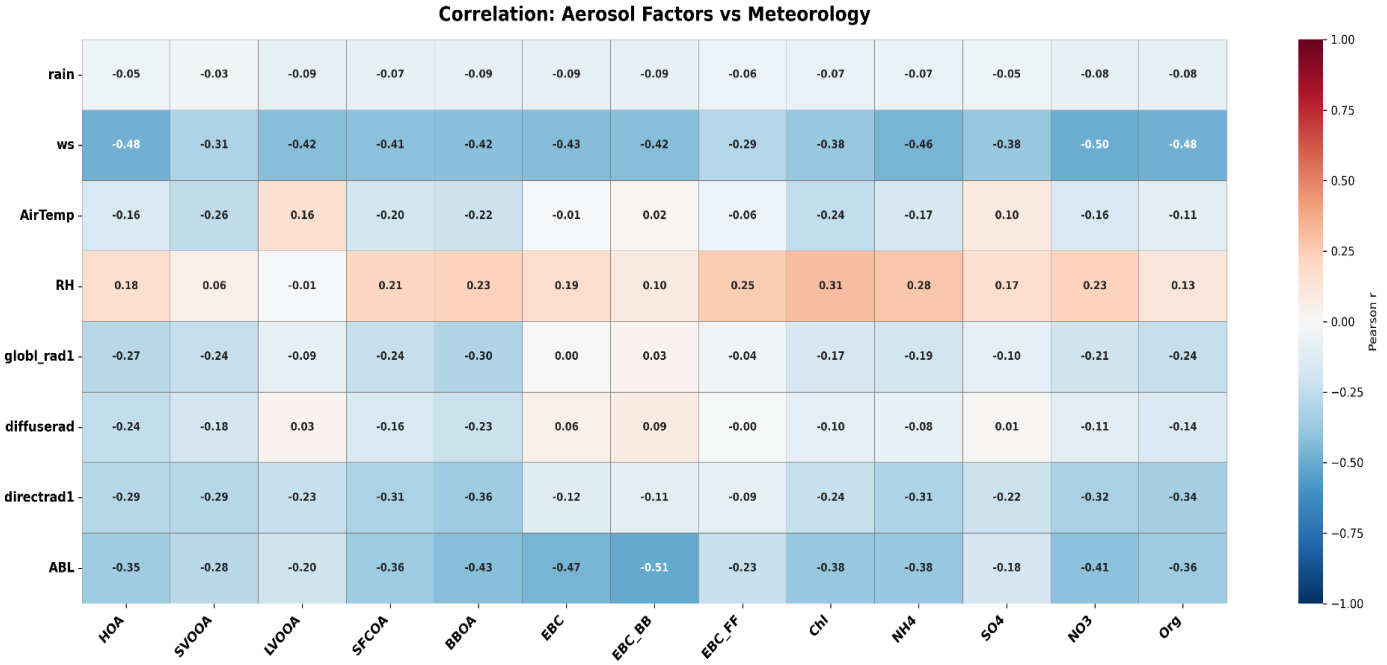

Figure S6: *Pearson correlation heatmap between aerosol factors (OA components, BC, and major inorganic species) and meteorological and radiative parameters. Positive and negative correlations indicate the influence of atmospheric dynamics and boundary-layer processes on aerosol variability.*

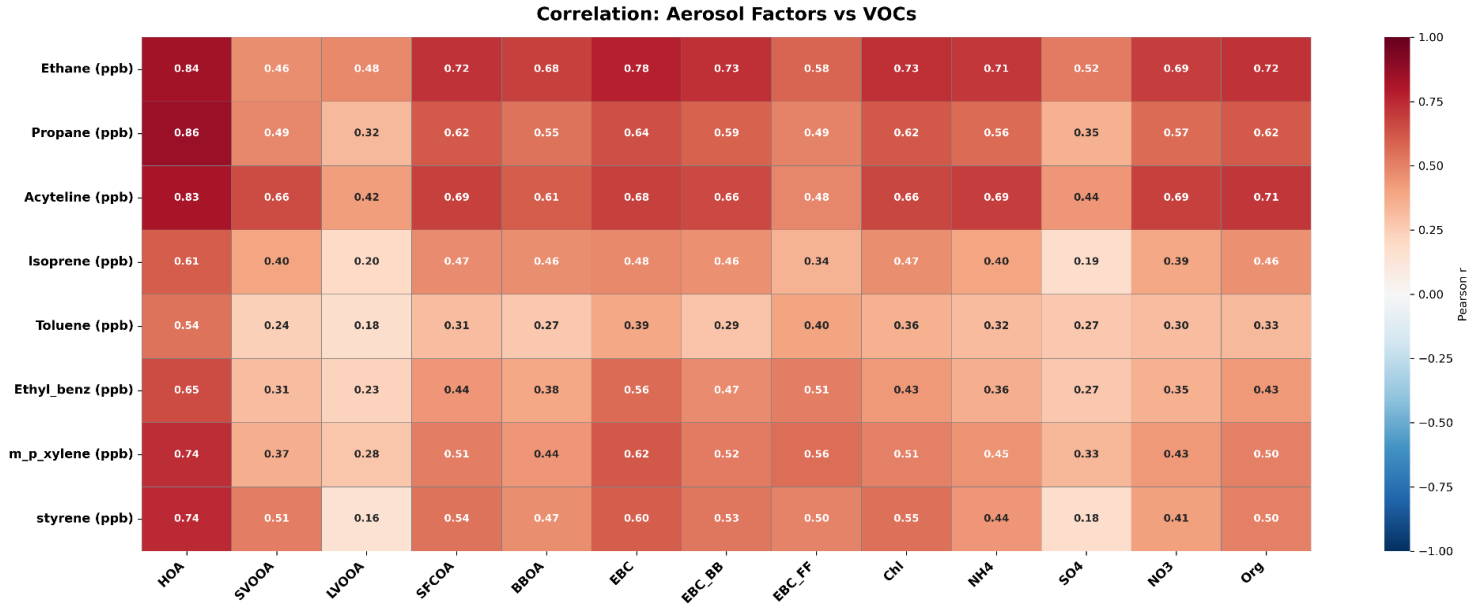

Figure S7: *Pearson correlation heatmap between aerosol factors (OA components, BC, and inorganic species) and measured volatile organic compounds (VOCs). Correlation patterns highlight potential source linkages and secondary formation pathways.*

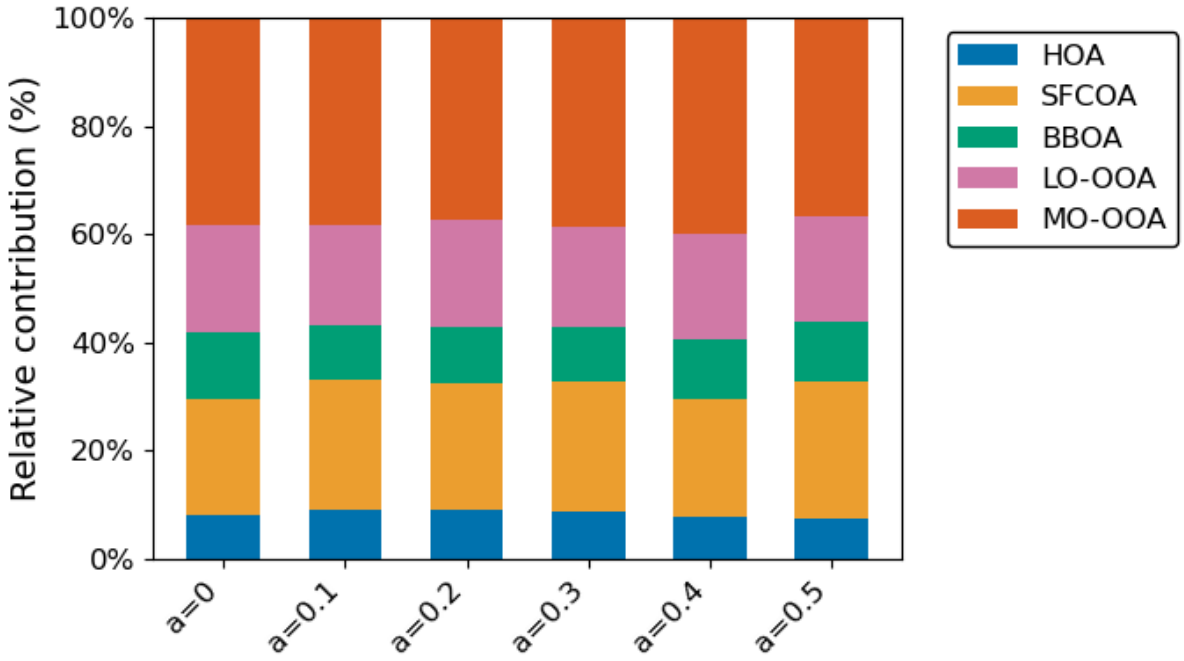

Figure S8: *Individual factor contribution for different a-value constrained run.*

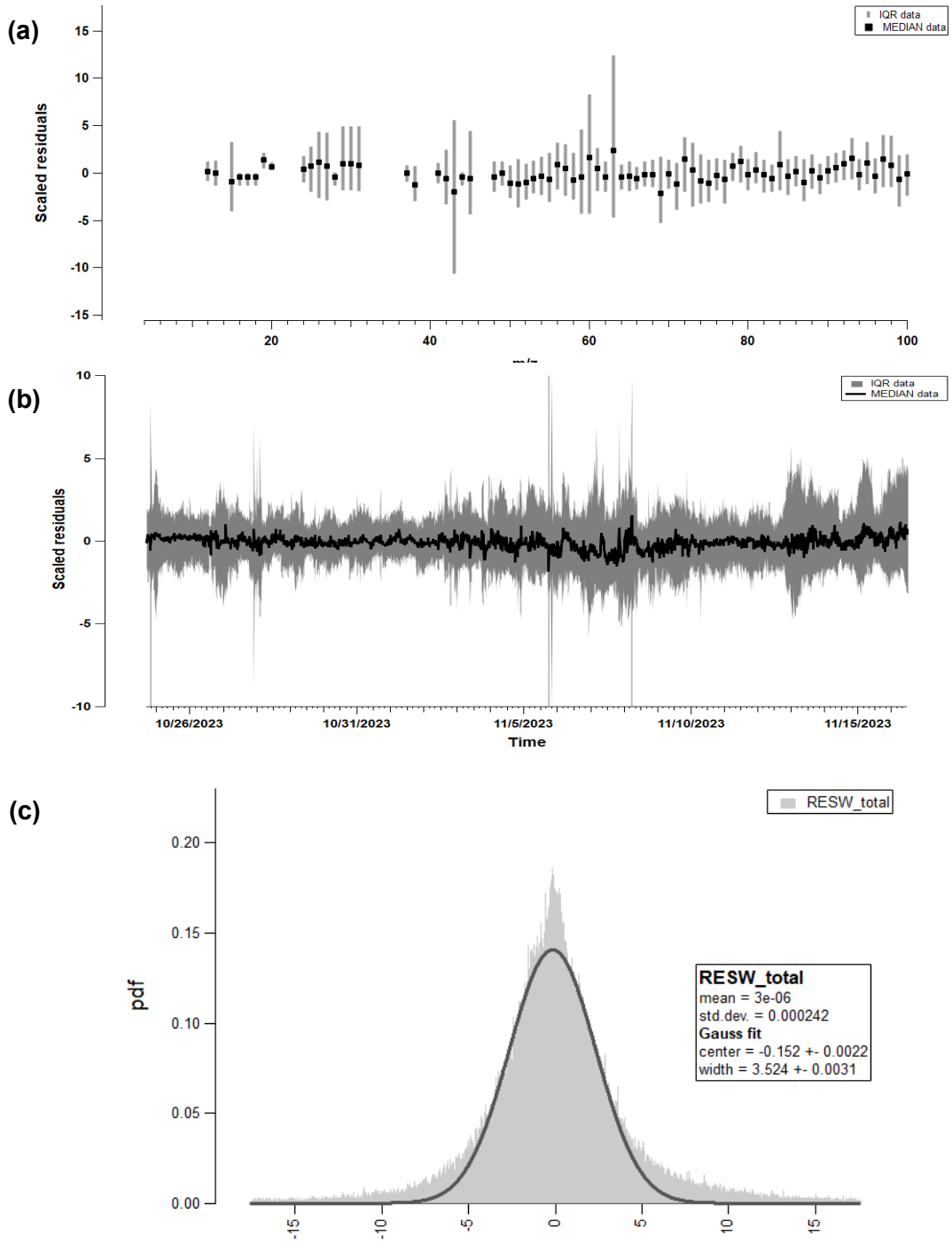

Figure S9: *Scaled residuals of the five-factor PMF solution as a function of (a) m/z and (b) time, and (c) their probability density function (PDF) fitted with a Gaussian curve. Black squares/line indicate the median scaled residuals, and grey bars or shaded areas represent the interquartile range (IQR).*

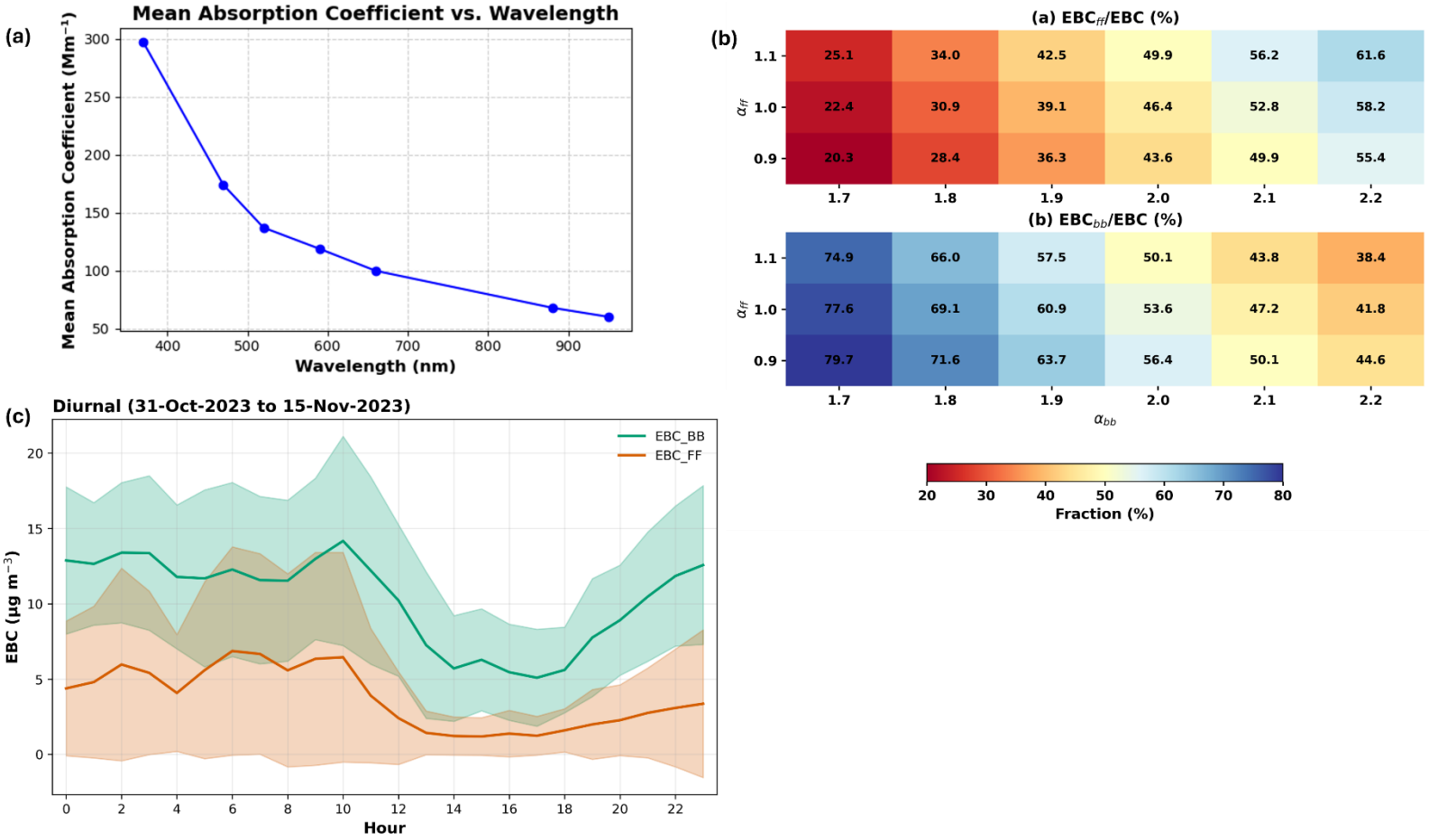

231 ***Figure S10:*** *(a) Spectral variation of the mean aerosol light absorption coefficient as a function of*
232 *wavelength. We can see stronger absorption in the UV region due to woodburning emissions in*
233 *intense agricultural activity. (b) Sensitivity of fossil-fuel black carbon (eBC_{ff}) and biomass-burning*
234 *black carbon (eBC_{bb}) fractional contributions to assumed absorption Ångström exponents (α_{ff} and*
235 *α_{bb}); color shading indicates percentage contribution. (c) Mean diurnal variation of eBC_{wb} and*
236 *eBC_{ff} concentrations during 31 October–15 November 2023, with shaded regions representing*
237 *variability (±1σ).*
238

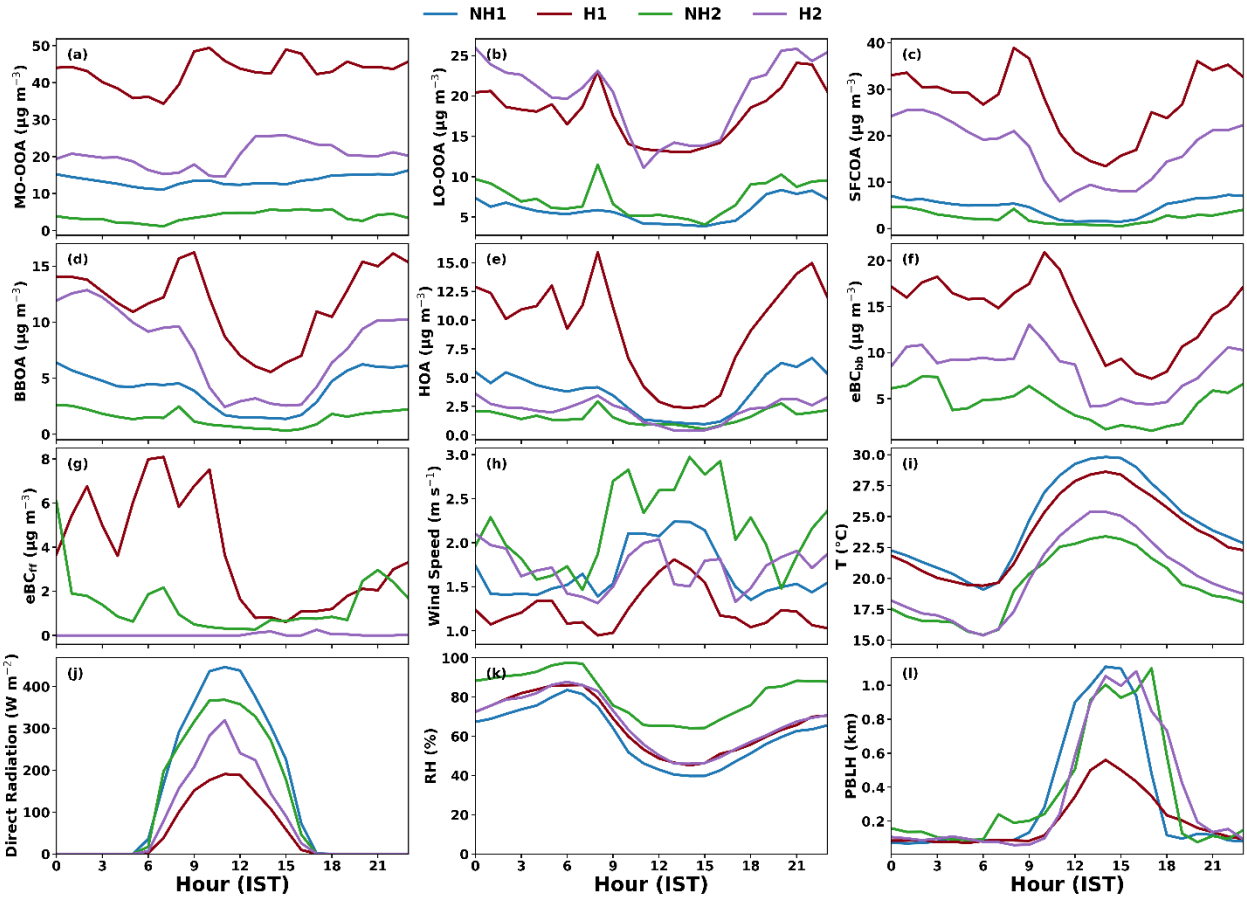

Figure S11: *Diurnal variation of PMF factors: HOA, LO-OOA, MO-OOA, SFCOA and BBOA; 2 resolved BC factors: eBC_{bb} and eBC_{ff} , meteorological parameters: Wind Speed, Temperature, Direct Radiation, Relative Humidity, PBLH during Haze (H1 & H2) and Non-Haze (NH1& NH2) period from 25th October 2023 to 15th November 2023.*

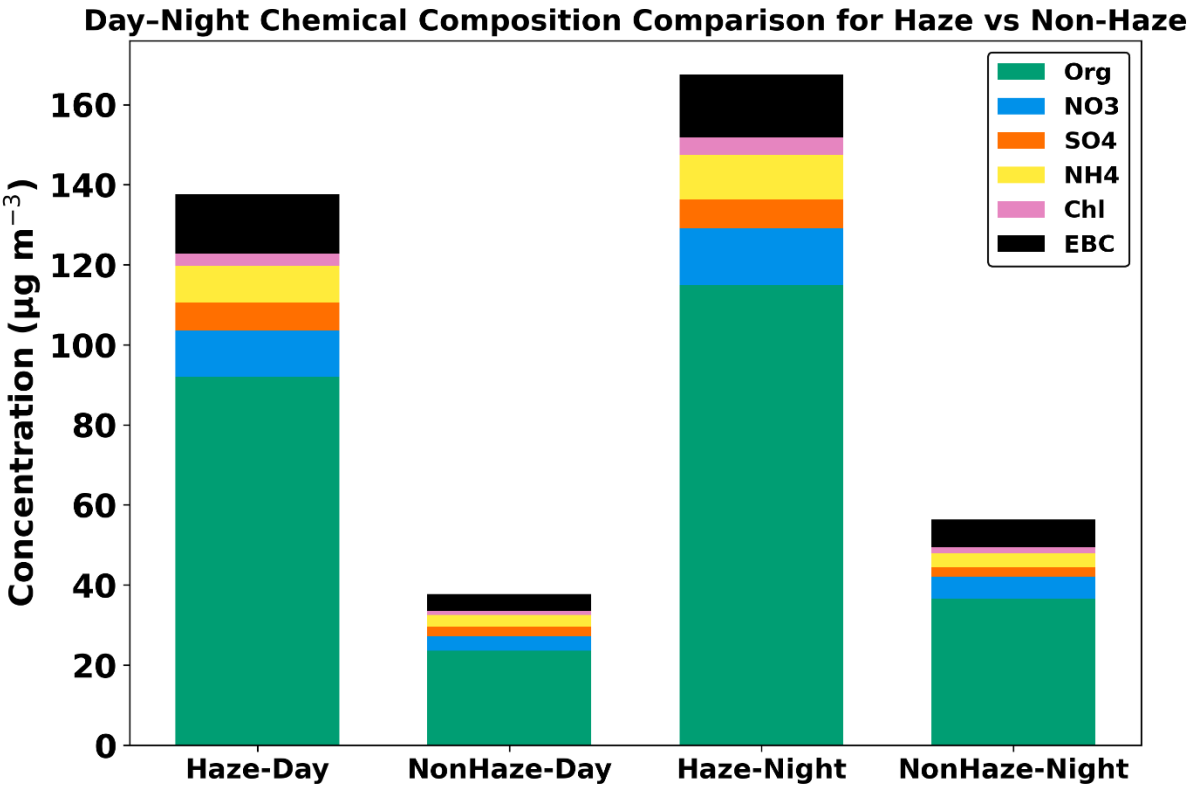

Figure S12: *Daytime and nighttime $PM_{2.5}$ chemical composition during haze and non-haze periods. Bars represent mean contributions of organic aerosol (Org), NO_3^-, SO_4^{2-}, NH_4^+, chloride (Chl), and equivalent black carbon (eBC). Data is for the full period from 25th October 2023 to 15th November 2023.*

252

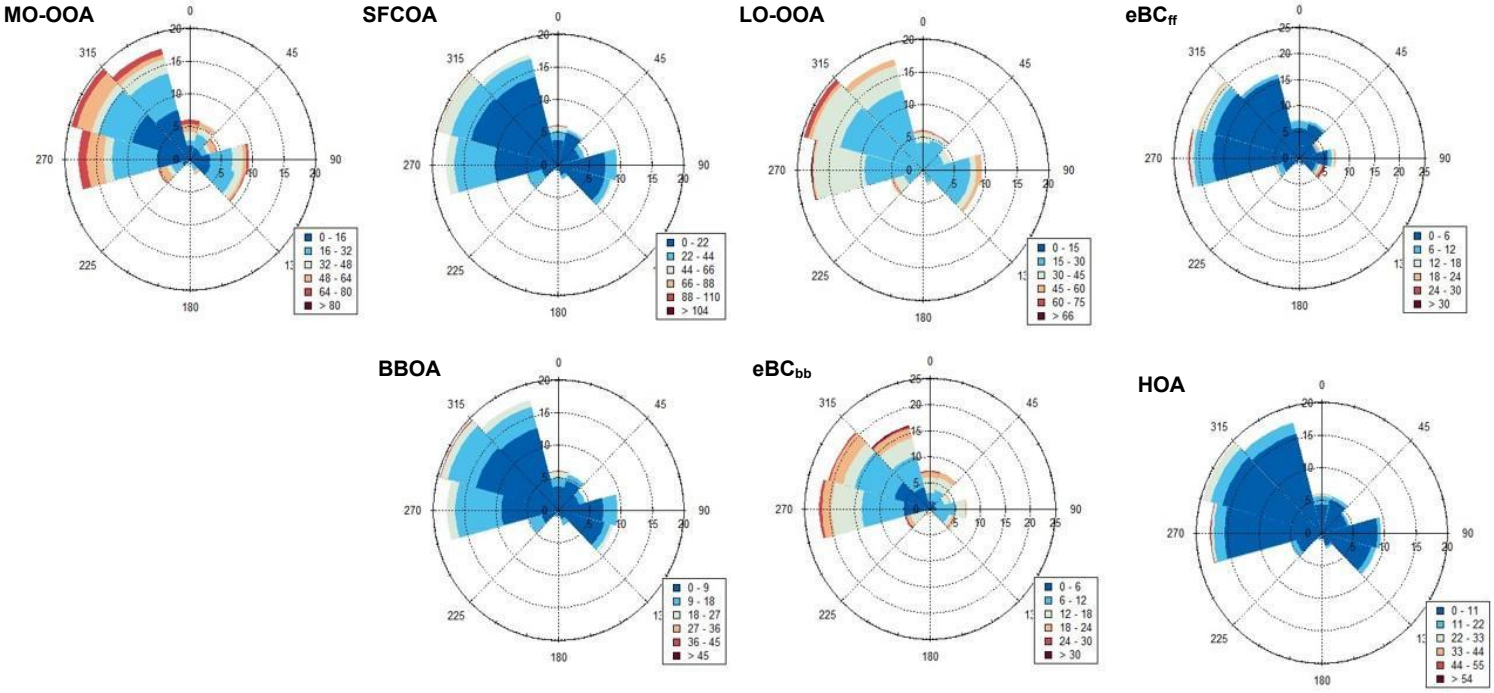

253 ***Figure S13:*** *Pollution Rose (PR) plots for full period of data from 25th October 2023 to 15th*
254 *November 2023 for 5 resolved OA factors: HOA, LO-OOA, MO-OOA, SFCOA and BBOA; 2 resolved*
255 *eBC factors: eBC$_{bb}$ and eBC$_{ff}$.*
256

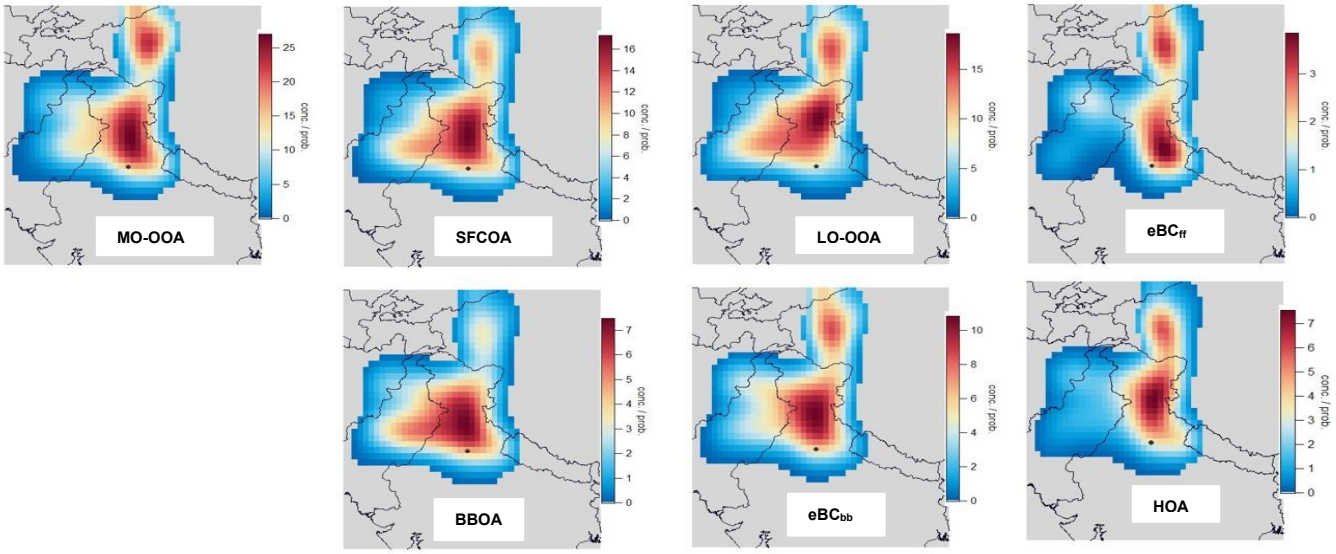

257 ***Figure S14:*** *Concentrated Weighted Trajectory (CWT) plots calculated with Hysplit Model for*
258 *period of data acquired from 25th October 2023 to 15th November 2023 for 5 resolved OA factors:*
259 *HOA, LO-OOA, MO-OOA, SFCOA and BBOA; 2 resolved eBC factors: eBC_{bb} and eBC_{ff}.*
260

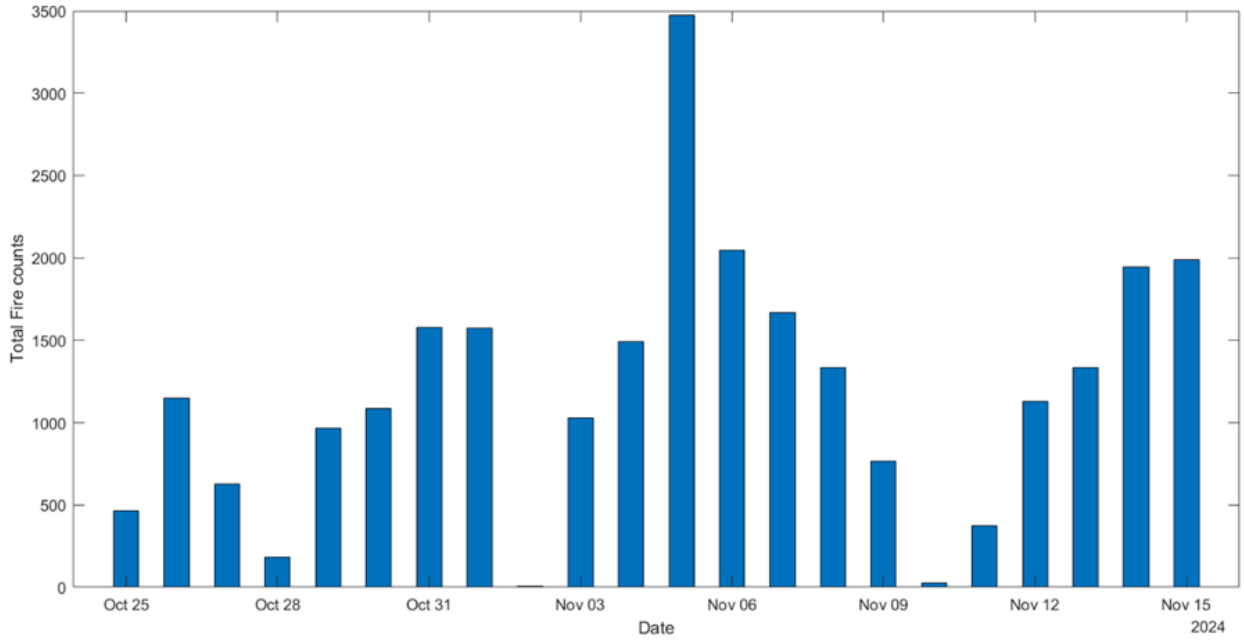

Figure S15: *Time series of the total fire counts obtained from SUOMI VIIRS.*

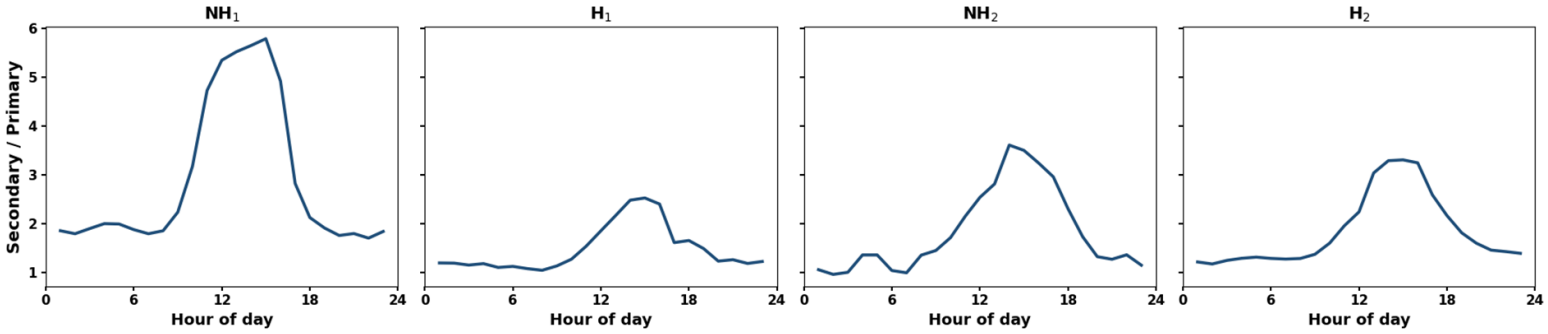

Figure S16: *Diurnal variation of the secondary-to-primary aerosol ratio during non-haze (NH_1, NH_2) and haze (H_1, H_2) periods. Higher ratios indicate enhanced secondary aerosol formation relative to primary emissions.*

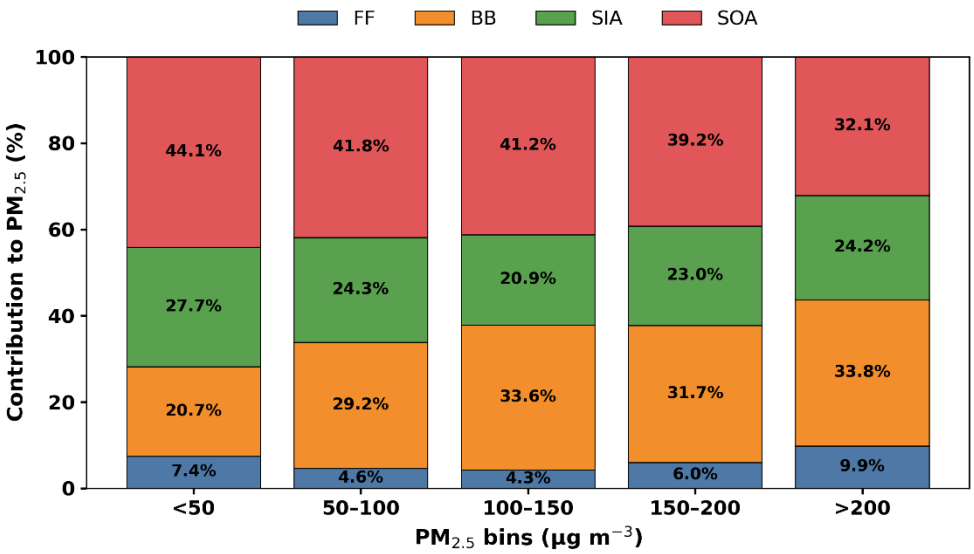

***Figure S17**: Variation in the chemical composition of particulate matter as a function of PM concentration. Bars show the percentage contribution of secondary organic aerosol (SOA), secondary inorganic aerosol (SIA), biomass-burning aerosol (BB), and fossil-fuel–related aerosol (FF) across different PM concentration bins.*

Where:

SOA = MO-OOA + LO-OOA

SIA = SO4 + NO3 + NH4 + Chl

BB = SFCOA + BBOA + EBC_{BB}

FF = HOA + EBC_{FF}

Table S1: *Elemental Ratio calculations(O:C, H:C and OM:OC) for 5 resolved OA factors: HOA, LO-OOA, MO-OOA, SFCOA and BBOA.*

Elemental Ratio	HOA	LO-OOA	MO-OOA	SFCOA	BBOA
f43	0.11	0.07	0.06	0.15	0.04
f44	0.01	0.21	0.27	0.05	0.01
O:C	0.1	0.72	0.91	0.21	0.09
H:C	1.19	1.09	1.04	1.25	0.96
OM:OC	1.3	2.1	2.34	1.45	1.28

Table S2: *Summary of different haze period data acquired from 25th October 2023 to 15th November 2023 for 5 resolved OA factors: HOA, LO-OOA, MO-OOA, SFCOA and BBOA; 2 resolved eBC factors: eBC_{bb} and eBC_{ff} . Arithmetic mean (AM), Geometric mean (GM), and Geometric standard deviation (GSD) for hourly concentrations are calculated.*

	Arithmetic Mean					***Geometric Mean (Std)***				
Variable	***Overall***	***NH1***	***H1***	***NH2***	***H2***	***Overall***	***NH1***	***H1***	***NH2***	***H2***
MO-OOA	*25*	*13.5*	*42.8*	*4.1*	*20.2*	*17.2 (2.7)*	*11.3 (2.0)*	*38.2 (1.7)*	*3.3 (2.1)*	*19.4 (1.3)*
LO-OOA	*12.8*	*5.8*	*18*	*7.3*	*20.4*	*9.6 (2.2)*	*5.3 (1.5)*	*14.0 (2.1)*	*6.6 (1.6)*	*19.6 (1.3)*
SFCOA	*15.1*	*4.6*	*27.5*	*2.4*	*17*	*7.0 (4.9)*	*2.4 (4.4)*	*22.4 (2.0)*	*1.4 (3.4)*	*15.0 (1.7)*
BBOA	*7.3*	*4*	*11.8*	*1.5*	*7.8*	*4.7 (2.9)*	*3.1 (2.2)*	*10.0 (1.9)*	*0.9 (2.8)*	*6.5 (1.9)*
HOA	*5.5*	*3.6*	*9.4*	*1.5*	*2.2*	*3.3 (2.8)*	*2.6 (2.3)*	*7.1 (2.2)*	*1.3 (1.9)*	*1.7 (2.4)*
eBC_{bb}	*10.9*	*---*	*14.2*	*4.2*	*8.3*	*8.9 (2.0)*	*---*	*13.1 (1.6)*	*3.4 (2.1)*	*7.6 (1.5)*
eBC_{ff}	*3.1*	*---*	*3.8*	*1.2*	*0.03*	*2.4 (4.3)*	*---*	*2.9 (3.9)*	*0.9 (3.4)*	*0.2 (2.5)*

Table S3: *Day time and Night time summary of different haze period data acquired from 25th October 2023 to 15th November 2023 for 5 resolved OA factors: HOA, LO-OOA, MO-OOA, SFCOA and BBOA; 2 resolved eBC factors: eBC_{bb} and eBC_{ff}. Arithmetic mean (AM) are calculated for all the factors.*

	Overall		***NH1***		***H1***		***NH2***		***H2***	
Variable	***Day***	***Night***	***Day***	***Night***	***Day***	***Night***	***Day***	***Night***	***Day***	***Night***
MO-OOA	*24.1*	*25.8*	*12.8*	*14.3*	*42.9*	*42.7*	*4.3*	*3.8*	*20*	*20.3*
LO-OOA	*10.6*	*15.1*	*4.7*	*6.9*	*15.6*	*20.2*	*5.9*	*9.1*	*16.6*	*23.7*
SFCOA	*11.8*	*18.5*	*3.1*	*6.2*	*23.4*	*31.2*	*1.4*	*3.6*	*12.2*	*21.2*
BBOA	*5.5*	*9.2*	*2.7*	*5.4*	*10*	*13.5*	*0.9*	*2.2*	*5*	*10.3*
HOA	*3.7*	*7.3*	*2.2*	*5.1*	*6.6*	*12*	*1.2*	*1.9*	*1.6*	*2.7*
eBC_{bb}	*10*	*11.7*	*--*	*--*	*13.6*	*14.8*	*3.6*	*5*	*7.7*	*8.8*
eBC_{ff}	*3.2*	*3*	*--*	*--*	*3.8*	*3.7*	*0.7*	*1.9*	*0.046*	*0.012*

Table S4: *Summary of different haze period data acquired from 25th October 2023 to 15th November 2023 for Primary Aerosol(PA): (HOA + SFCOA + BBOA + eBC_{ff} + eBC_{bb}) and Secondary Aerosols(SA): (LO-OOA + MO-OOA + Chl^- + NO_3^- + SO_4^{2-} + NH_4^+) . Arithmetic mean (AM), Geometric mean (GM), and Geometric standard deviation (GSD) for hourly concentrations are calculated.*

Period	*Aerosol Type*	*AM (µg/m^3)*	*GM (µg/m^3)*	*GSD*
NH1	*PA*	*12.22*	*8.57*	*2.53*
NH1	*SA*	*32.17*	*27.58*	*1.86*
H1	*PA*	*66.7*	*58.66*	*1.72*
H1	*SA*	*99.54*	*92.76*	*1.49*
NH2	*PA*	*10.71*	*8.91*	*1.91*
NH2	*SA*	*17.95*	*16.81*	*1.45*
H2	*PA*	*35.31*	*32.06*	*1.6*
H2	*SA*	*61.39*	*60.06*	*1.24*

Table S5: *Percentage contribution in different haze period data acquired from 25th October 2023 to 15th November 2023 for Primary Aerosol(PA): (HOA + SFCOA + BBOA + eBC_{ff} + eBC_{bb}) and Secondary Aerosols(SA): (LO-OOA + MO-OOA + Chl^{-} + NO_3^- + SO_4^{2-} + NH_4^+) .*

Period	*Primary Aerosol (%)*	*Secondary Aerosol (%)*
NH1	*27.5*	*72.5*
H1	*40.1*	*59.9*
NH2	*37.4*	*62.6*
H2	*36.5*	*63.5*

References:

Canagaratna, M. R., Jimenez, J. L., Kroll, J. H., Chen, Q., Kessler, S. H., Massoli, P., Hildebrandt Ruiz, L., Fortner, E., Williams, L. R., Wilson, K. R., Surratt, J. D., Donahue, N. M., Jayne, J. T., and Worsnop, D. R.: Elemental ratio measurements of organic compounds using aerosol mass spectrometry: characterization, improved calibration, and implications, Atmos. Chem. Phys., 15, 253–272, https://doi.org/10.5194/acp-15-253-2015, 2015.

Canonaco, F., Crippa, M., Slowik, J. G., Baltensperger, U., and Prévôt, A. S. H.: SoFi, an IGOR-based interface for the efficient use of the generalized multilinear engine (ME-2) for the source apportionment: ME-2 application to aerosol mass spectrometer data, Atmos. Meas. Tech., 6, 3649–3661, https://doi.org/10.5194/amt-6-3649-2013, 2013.

Canonaco, F., Tobler, A., Chen, G., Sosedova, Y., Slowik, J. G., Bozzetti, C., Daellenbach, K. R., El Haddad, I., Crippa, M., Huang, R.-J., Furger, M., Baltensperger, U., and Prévôt, A. S. H.: A new method for long-term source apportionment with time-dependent factor profiles and uncertainty assessment using SoFi Pro: application to 1 year of organic aerosol data, Atmos. Meas. Tech., 14, 923–943, https://doi.org/10.5194/amt-14-923-2021, 2021.

Chen, G., Canonaco, F., Slowik, J. G., Daellenbach, K. R., Tobler, A., Petit, J.-E., Favez, O., Stavroulas, I., Mihalopoulos, N., Gerasopoulos, E., El Haddad, I., Baltensperger, U., and Prévôt, A. S. H.: Real-Time Source Apportionment of Organic Aerosols in Three European Cities, Environ. Sci. Technol., 56, 15290–15297, https://doi.org/10.1021/acs.est.2c02509, 2022.

Crippa, M., El Haddad, I., Slowik, J. G., DeCarlo, P. F., Mohr, C., Heringa, M. F., Chirico, R., Marchand, N., Sciare, J., Baltensperger, U., and Prévôt, A. S. H.: Identification of marine and continental aerosol sources in Paris using high resolution aerosol mass spectrometry, JGR Atmospheres, 118, 1950–1963, https://doi.org/10.1002/jgrd.50151, 2013.

Hu, W., Day, D. A., Campuzano-Jost, P., Nault, B. A., Park, T., Lee, T., Croteau, P., Canagaratna, M. R., Jayne, J. T., Worsnop, D. R., and Jimenez, J. L.: Evaluation of the New Capture Vaporizer for Aerosol Mass Spectrometers (AMS): Elemental Composition and Source Apportionment of Organic Aerosols (OA), ACS Earth Space Chem., 2, 410–421, https://doi.org/10.1021/acsearthspacechem.8b00002, 2018.

Paatero, P. and Tapper, U.: Positive matrix factorization: A non-negative factor model with optimal utilization of error estimates of data values, Environmetrics, 5, 111–126, https://doi.org/10.1002/env.3170050203, 1994.

Ulbrich, I. M., Canagaratna, M. R., Zhang, Q., Worsnop, D. R., and Jimenez, J. L.: Interpretation of organic components from Positive Matrix Factorization of aerosol mass spectrometric data, Atmos. Chem. Phys., 2009.